ELSEVIER

Catalysis Today 77 (2002) 191–204

CATALYSIS TODAY

www.elsevier.com/locate/cattod

Co-support compound formation in Co/Al_2O_3 catalysts: effect of reduction gas containing CO

Bunjerd Jongsomjit[1], James G. Goodwin Jr.*

Department of Chemical Engineering, Clemson University, Clemson, SC 29634, USA

Abstract

The effect of the addition of CO during H_2 reduction on Co-support compound formation in a Co/γ-Al_2O_3 catalyst was investigated. It is known that such compound formation can occur during catalyst reduction, is facilitated by the presence of water vapor, and results in a less active catalyst. In this study, a H_2 flow containing CO (1–9 vol.%) was used for standard reduction. Water vapor was also added (3 vol.%) in one series of experiments in order to examine the impact of CO when relatively high partial pressures of water vapor are also present. After reduction at various conditions, the pretreated catalyst samples were characterized and CO hydrogenation ($H_2/CO = 10/1$, 220 °C, 1.8 atm) also performed. Both initial and steady-state rates during CO hydrogenation went through a maximum for the addition of 3–5 vol.% CO during standard reduction. The maximum rate was about four times that in the case where no CO was added. A similar trend was found even where reduction occurred with a high partial pressure of water vapor. It is concluded that the addition of CO during reduction has a significant effect on activity of the catalyst due to increases in both Co reducibility and dispersion.

Keywords: Reduction of Co catalysts; Co-support compound formation; Co FTS catalysts; CO hydrogenation

1. Introduction

Due to their high activities [1], high selectivities to linear hydrocarbons, and low activities for the water gas shift reaction [2,3], supported cobalt (Co) catalysts are considered to be the most important catalysts for Fischer–Tropsch synthesis (FTS) based on natural gas conversion. Since only reduced Co metal is active for FTS, it is known that Co-support compound formation (Co-SCF) can be one of the causes of catalyst deactivation. It has been reported that Co-SCF can occur under pretreatment and/or reaction conditions [4–17].

Water vapor is a byproduct of metal catalyst reduction and has also been shown to have a major impact on Co-SCF. In a previous study reported by our laboratory [6], water vapor was found to increase the amount of non-reducible (at temperatures <900 °C) Co "aluminate" formed during reduction of $Co–Ru/\gamma$-Al_2O_3. It was suggested that water vapor decreases the reducibility of the cobalt in possibly two ways: (i) inhibition of the reduction of well-dispersed CoO interacting with the alumina support possibly by increasing the cobalt–alumina interaction, and/or (ii) facilitation of the migration of cobalt ions into probable tetrahedral sites of γ-Al_2O_3 to form a non-reducible (at temperatures <900 °C) Co "aluminate". This irreversible Co "aluminate" formation results in a decrease in the amount of cobalt able to be reduced using conventional reduction procedures. However, it is uneconomic to decrease water vapor partial pressure to

* Corresponding author. Tel.: +1-864-656-3055; fax: +1-864-656-0784.
E-mail address: james.goodwin@ces.clemson.edu (J.G. Goodwin Jr.).
[1] Department of Chemical and Petroleum Engineering, University of Pittsburgh, Pittsburgh, PA 15261, USA.

0920-5861/02/$ – see front matter
PII: S0920-5861(02)00245-6

low enough levels during reduction of large amounts of Co catalysts for industrial scale processes to avoid facilitation of Co-SCF. Thus, in order to decrease the amount of non-reducible Co-SCF, a way needs to be found to minimize the impact of water vapor during reduction.

FTS at high conversions results in high partial pressures of water vapor as a byproduct without significant deactivation of Co catalysts. Thus, it is assumed that the presence of CO may help to prevent Co catalysts from rapidly deactivating due to Co-SCF. This paper reports the results of a study of the effect of CO partial pressure on Co-SCF during H_2 reduction of a Co/γ-Al_2O_3 catalyst. Since water vapor can have a significant impact on Co-SCF, the effect of CO on the H_2 reduction of Co/γ-Al_2O_3 at low and relatively high partial pressures of water vapor was investigated. Noble metal promotion of the Co/γ-Al_2O_3 was not used in this study in order to maximize the amount of Co-SCF [18].

2. Experimental

2.1. Materials

2.1.1. Co/γ-Al_2O_3

The Co/γ-Al_2O_3 catalyst was prepared by the incipient wetness impregnation of γ-Al_2O_3 having a specific surface area of 209 m^2/g and an average particle size ca. 60 μm. The support precursor (Vista B boehmite) was first calcined at 500 °C for 10 h before impregnation in order to put it in the form of γ-Al_2O_3. Cobalt nitrate [$Co(NO_3)_2{\cdot}6H_2O$] was dissolved in de-ionized water and impregnated into the support using incipient wetness to give a final catalyst with 20 wt.% cobalt. The catalyst was dried at 110 °C for 12 h and calcined in air at 300 °C for 2 h.

2.1.2. CoO, Co_3O_4 (spinel), and $CoAl_2O_4$ (spinel)

In order to identify the XRD peaks and Raman bands of the samples, cobalt (II) oxide [95% CoO] from Alfa Aesar, cobalt (II, III) oxide (spinel) [99.5% Co_3O_4] from Strem Chemicals, Inc., and cobalt aluminate (spinel) [98% $CoAl_2O_4$] from Alfa Aesar were used as reference materials.

2.2. Catalyst pretreatment

Standard reduction of the calcined catalyst was carried out in a fixed-bed flow reactor under differential conditions at 1 atm using a temperature ramp from ambient to 350 °C at 1 °C/min and holding at 350 °C for 10 h in a gas flow having a space velocity of 16,000 h^{-1} and consisting of H_2 or a mixture of H_2 and 3 vol.% added water vapor. Various amounts of CO between 0 and 9 vol.% (P_{CO}/P_{H_2} = 0–0.10) were also introduced into the reduction gas from the beginning. The reduced catalyst was then passivated at room temperature for 2 h with a mixture of O_2/He (5.2% of O_2). The high space velocity of the H_2 flow when water vapor was not added insured that the partial pressure of water vapor in the catalyst bed produced by Co oxide reduction would be essentially zero in that case.

2.3. Catalyst nomenclature

The nomenclature used for the catalyst samples in this study is the following:

- Co–R: the catalyst samples reduced in H_2.
- Co–R[W]: the catalyst samples reduced in a mixture of H_2 with 3% water vapor added.
- Co–R[C-*n*]: the catalyst samples reduced in H_2 and *n*% (1–9%) of CO.
- Co–R[WC-*n*]: the catalyst samples reduced in a mixture of H_2 with 3% added water vapor and *n*% (1–9%) of CO.

2.4. Catalyst characterization

2.4.1. X-ray powder diffraction (XRD)

XRD was performed to determine the bulk crystalline phases of the catalyst samples following different reduction conditions and passivation. XRD patterns of samples were collected using a Scintag XDS-2000 X-ray diffractometer with monochromatized Cu Kα radiation (λ = 1.54439 Å). The spectra were scanned at a rate of 2.4°/min from $2\theta = 20°$ to 80°.

2.4.2. Raman spectroscopy

The Raman spectra of the samples were collected by projecting a continuous wave laser of helium–neon (He–Ne) red (632.816 nm) through the samples exposed to air at room temperature. A scanning range

between 100 and 1000 cm^{-1} with a resolution of 2 cm^{-1} was applied. The data were analyzed using Renishaw Windows-based Raman Environment (WiRE) software which allows Raman spectra to be captured, calibrated, and analyzed using system 2000 functionality via the Galactic GRAMS interface with global imaging capacity.

2.4.3. SEM and EDX

SEM and EDX were performed to study the morphologies of the catalyst samples and elemental distributions, respectively. A Hitachi S3500N SEM was used in the back scattering electron (BSE) mode at 15 kV with a working distance (the distance between a sample and the electron beam) of 15 mm. After the SEM micrographs were taken, EDX was performed to determine the elemental concentration on the catalyst surface (using INCA software).

2.4.4. Hydrogen chemisorption

Static H_2 chemisorption on the re-reduced cobalt catalyst samples was used to determine the number of reduced surface cobalt metal atoms. This is related to the overall activity of the catalyst during FTS. Gas volumetric chemisorption at 100 °C was performed using the method described by Reuel and Bartholomew [19]. Chemisorption was conducted in a Micromeritics ASAP 2010 using ASAP 2010C V3.00 software. Prior to H_2 chemisorption, the passivated catalyst samples were evacuated to 10^{-6} mm Hg at 100 °C for 15 min, reduced in H_2 flow at 100 °C for 15 min, reduced at 350 °C for 10 h, and then evacuated at 350 °C for 90 min to desorb any hydrogen.

2.4.5. Temperature programmed reduction (TPR)

TPR was performed to determine the reducibility and reduction behavior of the catalyst samples. TPR was carried out in an Altamira AMI-1 system using 50 mg of catalyst and a temperature ramp from 30 to 900 °C at 5 °C/min. The reduction gas was 5% H_2 in Ar. A cold trap (−70 °C) was placed before the detector to remove water produced during the reaction. A thermal conductivity detector (TCD) was used to determine the amount of hydrogen consumed. The amount of hydrogen consumption was calibrated using TPR of silver oxide (Ag_2O) at the same conditions. The reduced and passivated catalyst samples were re-calcined in situ at 300 °C for 2 h before performing TPR.

2.5. Reaction

The catalyst samples reduced with various reduction gas compositions were tested for their initial and steady-state activity. Hydrogenation of CO was carried out at 220 °C and 1.8 atm. A flow rate of H_2/CO/He = 20/2/8 cm^3/min in a fixed-bed flow reactor under differential conditions was used. A relatively high H_2/CO ratio was used to minimize deactivation due to carbon deposition during reaction. Thermocouples at the top and at the bottom of the catalyst bed assured precise temperature control during pretreatment and reaction. Typically, 15 mg of a reduced and passivated catalyst sample was re-reduced in situ in flowing H_2 (30 cm^3/min) at 350 °C for 10 h prior to the reaction. Reactor effluent samples were taken at 1 h intervals and analyzed by GC. In all cases, steady-state was reached within 5 h.

3. Results

3.1. XRD

XRD patterns for representative catalyst samples reduced at various reduction gas phase compositions are shown in Fig. 1. Reference patterns for γ-Al_2O_3, CoO, Co_3O_4 (spinel), and $CoAl_2O_4$ (spinel) are also shown. The XRD results for all the catalyst samples reduced with the various gas compositions used in this study were identical after passivation. For all the samples, only XRD peaks of CoO at 37°, 42.6° and 61.8° as well as those for γ-Al_2O_3 were evident. No XRD peaks of $CoAl_2O_4$ (spinel) were detected for any of the catalyst samples.

3.2. Raman spectroscopy

Raman spectra of the catalyst samples are shown in Figs. 2–4. Raman bands for all Co–R[C-*n*] were identical and different from that for Co–R as shown in Fig. 2. Only two very broad Raman bands at ca. 690 and 560 cm^{-1} were detected for Co–R and this has been correlated to the formation of a highly dispersed Co “aluminate” [18]. Strong Raman bands at 690 and

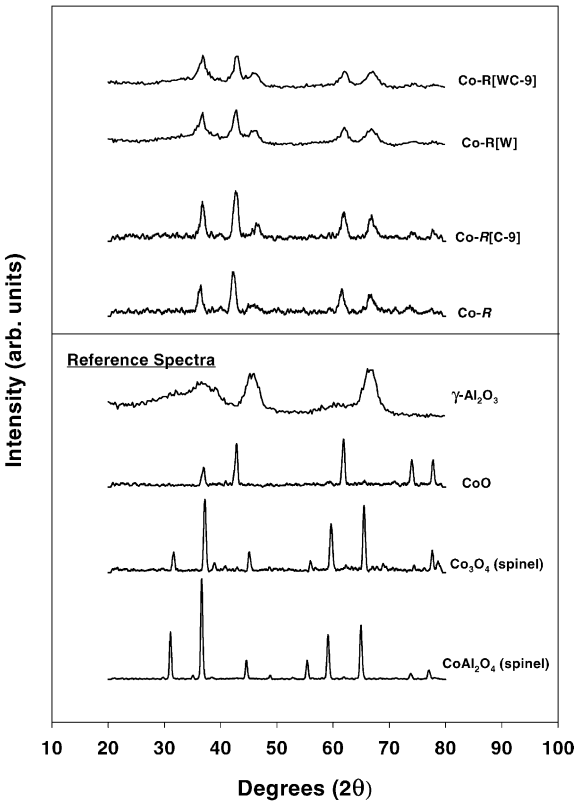

Fig. 1. XRD patterns of Co/γ-Al_2O_3 after various reduction conditions, $CoAl_2O_4$ (spinel), Co_3O_4 (spinel), CoO, and γ-Al_2O_3.

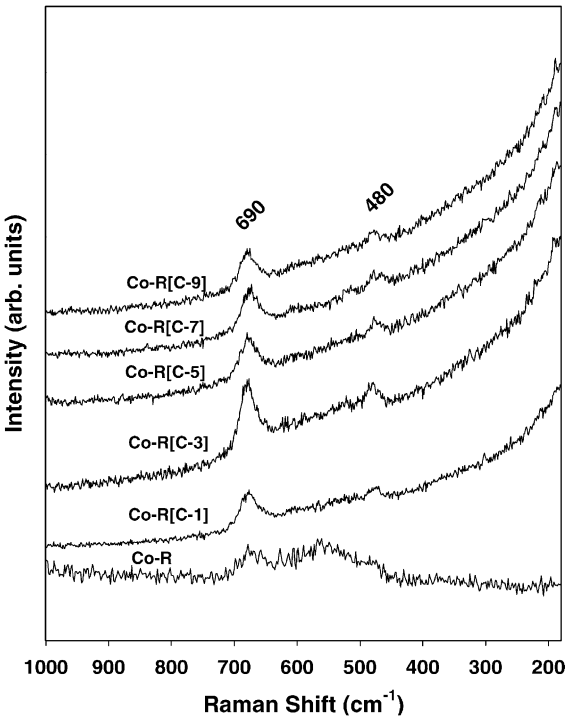

Fig. 2. Raman spectra of Co–R and Co–R[C-*n*] samples.

480 cm^{-1} were observed for the Co–R[C-*n*] samples. As can be seen in Fig. 3, as previous reported [18], the addition of water vapor during reduction resulted in an enhancement for Co–R[W] of the Co "aluminate" bands, without any other bands being evident. However, for the Co–R[WC-9] sample at the highest concentration of added CO, there were obvious Raman bands at 690, 619, 519, 480, and 198 cm^{-1}. These bands can be assigned to Co_3O_4 (see Fig. 4) present on catalyst surface after the samples were exposed to air rather than CoO (detected in the bulk by XRD) since Raman is more of a surface technique. Samples reduced at lower concentrations of CO also exhibited similar peaks as well as a broad peak from 520 to 620 cm^{-1} that obscured the weak bands at 619 and 519 cm^{-1}. The broad Raman band between 450 and 620 cm^{-1}, which represents Co "aluminate" as seen for Co–R[W], was thus apparently present for the Co–R[WC-*n*] samples where $n \leq 7$. No peaks for $CoAl_2O_4$ (spinel) were detected in any of the samples.

3.3. SEM and EDX

There was no significant change in morphology of the catalyst samples after the various reduction conditions used in this study. The typical morphology of a sample is shown in Fig. 5a and b. In all figures, the white or light spots represent high concentrations of Co and its compounds and the gray areas represent the alumina support with no/minimal Co. Fig. 5a shows the external surface of a catalyst granule of sample Co–R[C-9], whereas Fig. 5b shows a cross-section of a catalyst granule of the same sample. Co patches were well distributed over the external surface and throughout the interior of all the catalyst granules.

EDX gave useful information about elemental distribution in the pretreated catalyst granules. EDX mapping indicated that all elements in the catalyst samples were well distributed (Fig. 6 shows typical elemental distributions for a cross-section of a catalyst granule).

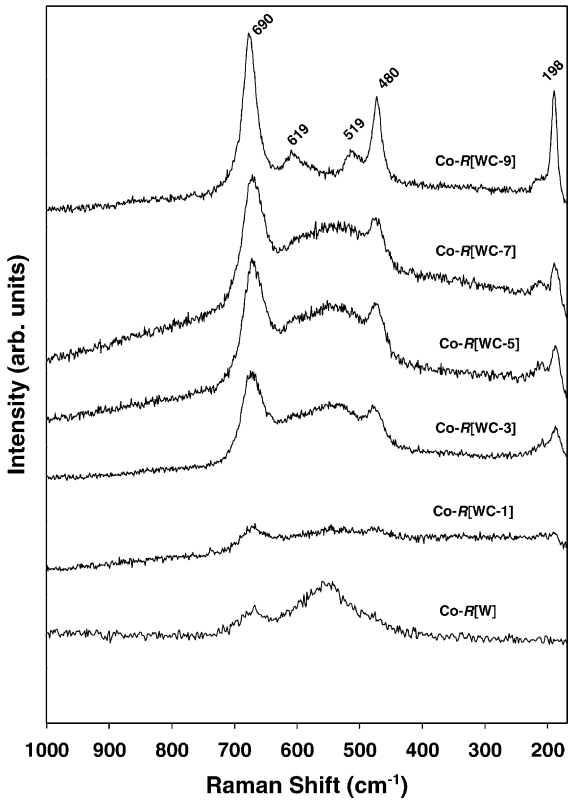

Fig. 3. Raman spectra of Co–R[W] and Co–R[WC-*n*] samples.

EDX was also able to detect the presence of carbon for those samples exposed to CO addition >3 vol.%. Average elemental compositions on the external catalyst granule surfaces of the samples are given in Table 1.

3.4. TPR

TPR was preformed to determine the reduction behavior and reducibility of the catalysts. TPR profiles of the catalyst samples after various pretreatment conditions are shown in Figs. 7 and 8. Reduction was observed for all catalyst samples to occur in two major peaks. The first peak is due to a two-step reduction of Co_3O_4 (with no/minimal interaction with the support) to Co metal [18,20–23] and occurred at ca. 320 °C for both Co–R[C-*n*] and Co–R[WC-*n*] samples. This peak occurred about 20 °C lower than those for Co–R and Co–R[W]. The second observable peak (very broad and made up of multiple overlapping peaks) is due to the reduction of Co species strongly interacting with the support [18,20–23] and occurred between 400 and 700 °C (max. at 650 °C) for both Co–R[C-*n*] and Co–R[WC-*n*] samples. The reducibilities (at temperatures up to 900 °C) of the catalysts were calculated and are given in Table 2. The reducibilities for TPR between 30 and 400 °C (related to the reducibilities of the samples during standard reduction at 350 °C [6]) ranged between 16 and 29% for Co–R[C-*n*] samples and 14–20% for Co–R[WC-*n*] samples. For Co–R[C-*n*], reducibility increased from 17% (for Co–R) up to a maximum of 29% for 5 vol.% added CO before decreasing when greater amounts of CO were added. For Co–R[WC-*n*], reducibility appeared to also go through a maximum (for 3–5 vol.% CO) with increasing amount of added CO, but the difference was less dramatic (14–20%). The results for reducibilities during TPR from 30 to 900 °C for the

Table 1
Elemental concentrations from EDX for the external surface of the catalyst granules after reduction at different gas phase compositions

Catalyst samples	Average elemental concentration (wt.%)[a]				
	C	O	Al	Co	Total
Co–R[C-1]	–	42.1	39.8	18.1	100
Co–R[C-3]	0.9	45.7	34.6	18.8	100
Co–R[C-5]	1.2	44.1	34.5	20.2	100
Co–R[C-9]	2.5	41.2	38.2	18.1	100
Co–R[WC-1]	–	47.0	32.4	20.6	100
Co–R[WC-3]	–	37.1	43.1	19.8	100
Co–R[WC-5]	0.7	42.8	35.6	20.9	100
Co–R[WC-7]	0.7	44.9	33.2	21.2	100
Co–R[WC-9]	1.5	40.9	35.5	22.1	100

[a] EDX was performed for the external surface of a catalyst sample and the average elemental concentrations were calculated based on elemental concentrations at 20 spots on a catalyst granule.

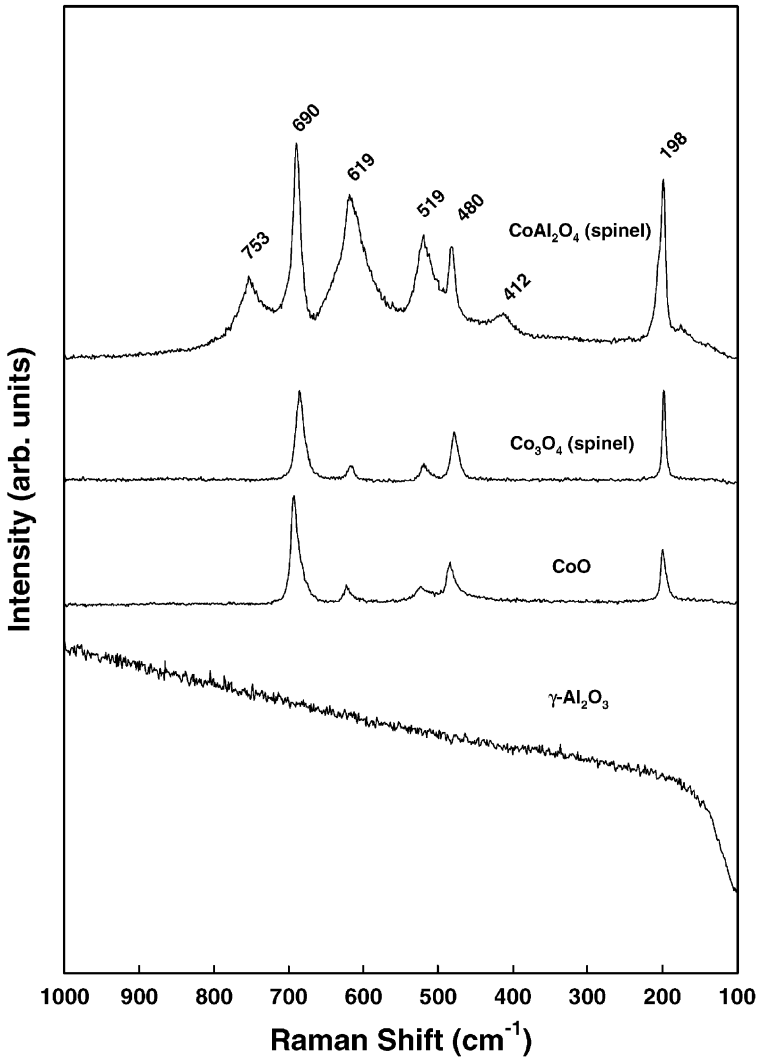

Fig. 4. Reference Raman spectra of γ-Al_2O_3, CoO, Co_3O_4 (spinel), and $CoAl_2O_4$ (spinel).

two catalyst sample series manifested similar trends as for 30–400 °C, but were greater.

3.5. H_2 chemisorption

H_2 chemisorption was performed to determine the overall Co metal dispersion after different reduction conditions. The Co metal dispersions of the samples are shown in Table 2 and ranged from 2.8 to 7.9%. For Co–R[C-*n*] samples, the Co metal dispersion increased from 3.2 to 7.9% with increasing CO concentration up to the maximum investigated of 9 vol.%. However, Co metal dispersion for the Co–R[WC-*n*] samples passed through a maximum of 6.2% for 3 vol.% added CO.

3.6. Reaction

CO hydrogenation (H_2/CO = 10/1) was performed to determine the overall activity of the catalyst samples reduced at various reduction gas compositions. The results are shown in Table 3 and Fig. 9 (no water

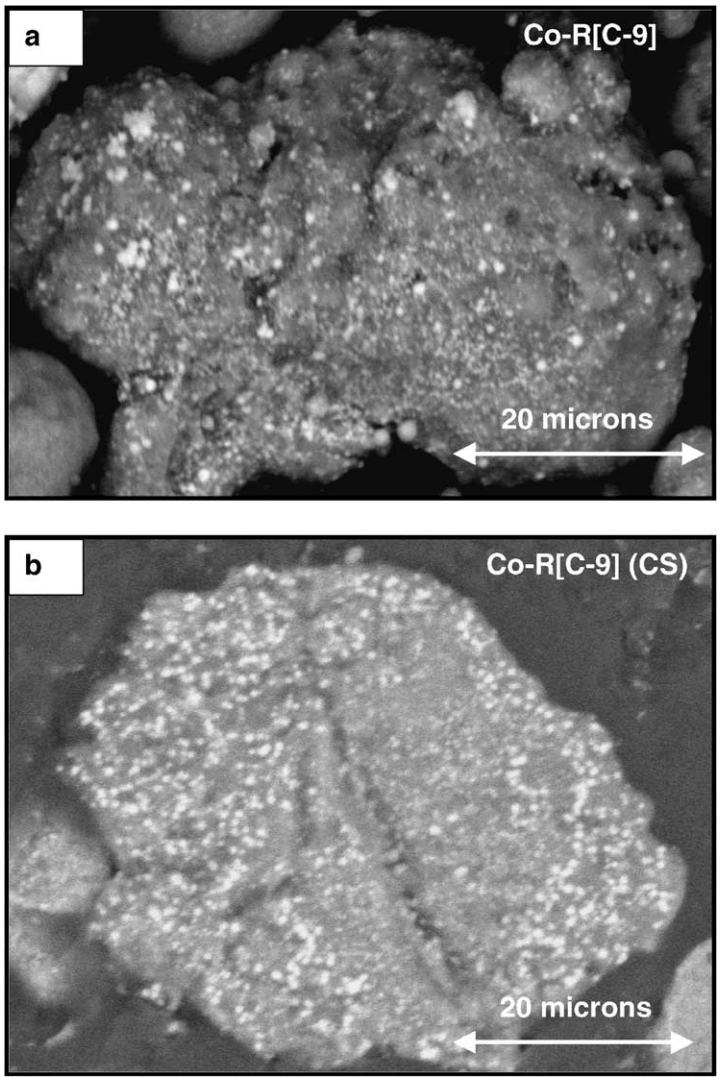

Fig. 5. (a) SEM micrographs of a typical granule of Co–R[C-9]; (b) SEM micrographs of the cross-sectional (CS) area of a catalyst granule of Co–R[C-9].

vapor added during reduction) and Fig. 10 (with water vapor added during reduction). It can be seen that for Co–R[C-*n*], the addition of CO during standard reduction of the Co catalyst caused the rate (both initial and steady-state) of CO hydrogenation to go through a maximum for the case of 5 vol.% CO addition. However, the rate after the addition of 9 vol.% CO during reduction was lower than that of Co–R, the base case.

A similar trend was found for Co–R[WC-*n*], except the maximum rate occurred after 3 vol.% CO addition and the rate after 9 vol.% CO addition was still significantly higher than for Co–R[W]. The selectivity to CH_4 during CO hydrogenation was found to be ca. 80–90%. Although the Co–R[C-*n*] results would appear to suggest that the CH_4 selectivity went through a minimum with CO addition during reduction, the Co–R[WC-*n*] results suggest little variation in selectivity. At this time, we are not prepared to conclude that there was any significant difference in selectivity for any of the samples.

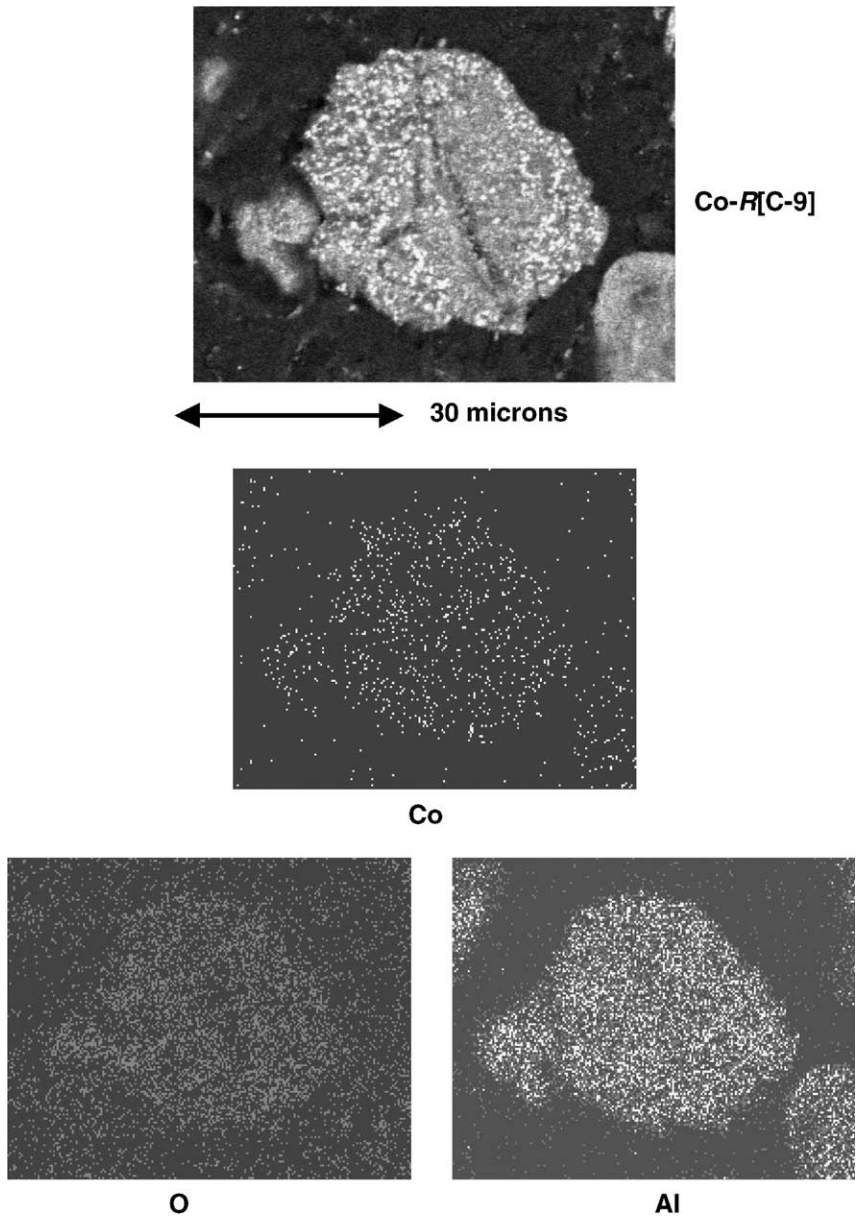

Fig. 6. Elemental distribution obtained by EDX mapping of a catalyst granule cross-section of Co–R[C-9].

4. Discussion

The addition of CO during standard reduction had a significant impact on the reaction rate during CO hydrogenation (H_2/CO = 10/1). It was found that an optimal concentration of CO (3–5 vol.%) added to H_2 during reduction at low or high partial pressures of water vapor produced specific activities four times greater than when the catalyst was reduced without CO addition (Figs. 9 and 10). One thing that might explain higher activity is increased reducibility.

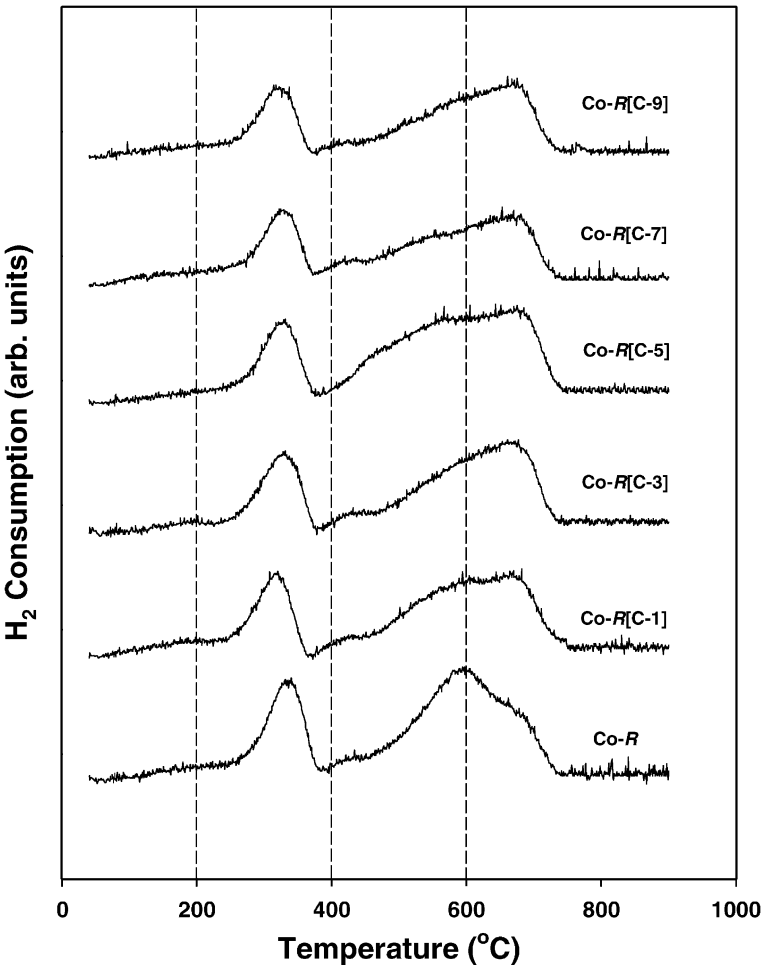

Fig. 7. TPR profiles of Co–R and Co–R[C-*n*] samples.

It is known that three reduction peaks located at ca. 200, 300 °C, and between 400 and 750 °C (max. at 600 °C) can be seen for calcined Co/γ-Al_2O_3 (calcined at 300 °C for 2 h) [18,20]. The first peak at ca. 200 °C has been assigned to the decomposition of residual Co nitrate. The second peak at ca. 300 °C has been assigned to the reduction of Co_3O_4 to CoO and Co^0 and the highest reduction temperature peak is related to the reduction of Co species strongly interacting with the alumina support to Co metal. Due to the sequential pretreatments (calcination, reduction, passivation, and recalcination) prior to TPR measurement, only two reduction steps are observed during TPR from 30 to 900 °C (Figs. 7 and 8) of the samples. The pretreatments used prior to TPR measurement were able to decompose all residual Co nitrate resulting in the absence of a peak at 200 °C. Based on the similar TPR profiles in this study, it is suggested that CO addition during reduction did not have a significant impact on the reduction characteristics (peak locations) of the samples with the possible exception of an increase in the kinetics of reduction for the peak ca. 340 °C that was shifted −20 °C. However, the % reducibilities were much more dramatically affected by the CO addition.

It was observed that, for standard reduction at low partial pressure of water vapor (Co–R[C-*n*]), the reducibility of this Co catalyst went through a maximum

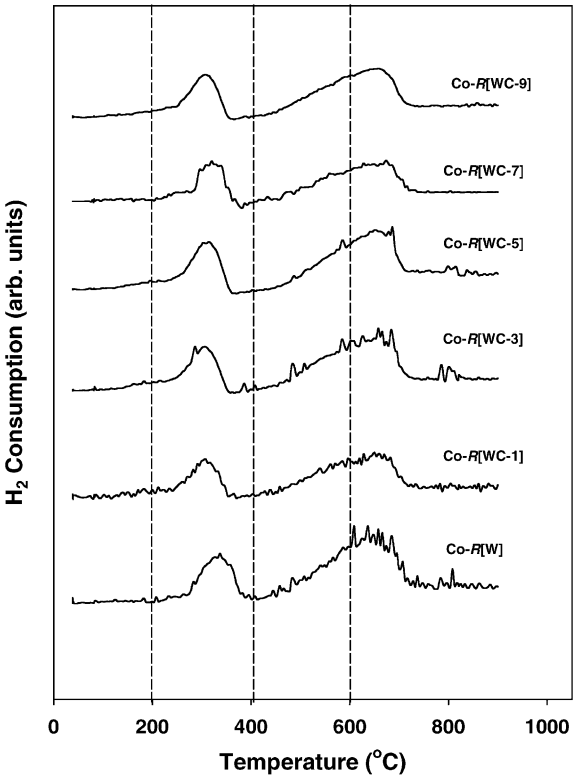

Fig. 8. TPR profiles of Co–R[W] and Co–R[WC-*n*] samples.

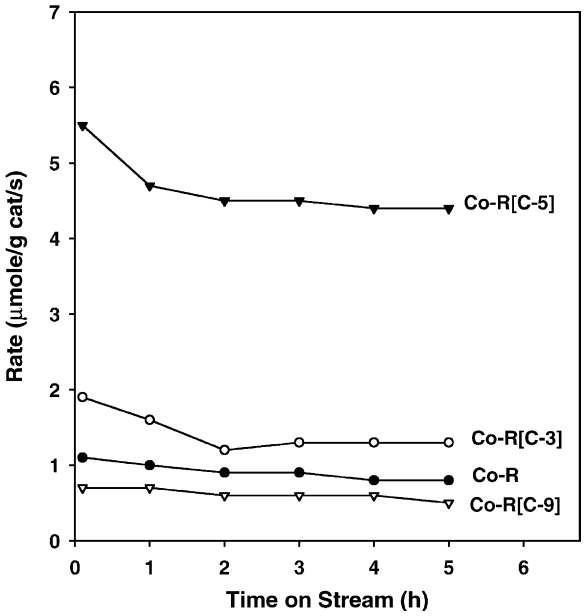

Fig. 9. Effect on reaction rate of CO addition during reduction at low partial pressures of water vapor.

with increasing amount of CO added during reduction. For reduction at high partial pressure of water vapor (Co–R[WC-*n*]), the results were much less dramatic, probably due to the impact of water vapor, but similar. It is possible that the addition of an optimum amount of CO resulted in an increase in reducibility due to CO helping to prevent the formation of Co species strongly interacting with the support. However, higher concentrations of CO possibly resulted in lower reducibilities as a result of H_2 being more difficult to activate on carbon-blocked Co surfaces and Co oxide being more difficult to reduce under deposited carbon (Table 1), especially graphitic carbon.

It is known that cobalt carbide can be formed during carburization of cobalt metal using CO [24]. However, there was no evidence of carbide formation, possibly due to the very high ratio of H_2/CO used. In this study, after the use of high concentrations of CO, it is not surprising that carbon deposition was found (Table 1). The amount of deposited carbon increased with increasing amount of CO added during reduction. However, for the same amount of CO added, there was less carbon deposited when water vapor was also added. This would appear to be due to an impact of water vapor on CO dissociation. The carbon deposited can exist in two forms: active carbon and graphite. Active carbon can react with hydrogen to form methane (CH_4) or oxygen to form CO or CO_2, whereas graphite is very non-reactive and difficult to remove.

If the deposited carbon were in the form of active carbon, it could have reacted with H_2 resulting in an increase in the amount of H_2 consumed during TPR. In order to determine the impact of this on the % reducibility obtained, the Co–R[C-9] and Co–R[WC-9] samples were analyzed for carbon content (Table 4). Both samples were chosen based on the fact that they contained the highest amount of carbon. After reduction and passivation, the carbon content was found to be ca. 0.9 and 0.6 wt.%, respectively. After re-reduction and passivation, only ca. 0.4 and 0.2 wt.% remained (57–64% of the carbon was removed). However, after recalcination prior to TPR measurement, the carbon content was found to be ca.

Table 2
TPR and H_2 chemisorption results for reduced Co/γ-Al_2O_3 at various reduction gas phase compositions

Catalyst samples	Reduction conditions			Reducibility (%)[a,b,c]		Total H_2 chemisorption (μmol H_2/g_{cat})[d]	Overall Co metal dispersion (%)[e]	Co^0, d_p (nm)[f]
	P_{CO}/P_{H_2} (at feed)	Added CO (vol.%)	P_{H_2O}/P_{H_2} (at feed)	30–900 °C[g]	30–400 °C			
Co–R	0	0	0	58	17	54	3.2	26
Co-R[C-1]	0.01	1	0	62	17	85	5.0	17
Co-R[C-3]	0.03	3	0	80	28	117	6.9	12
Co-R[C-5]	0.05	5	0	93	29	120	7.1	12
Co-R[C-7]	0.07	7	0	96	25	132	7.8	11
Co-R[C-9]	0.10	9	0	61	16	134	7.9	11
Co-R[W]	0	0	0.03	50	14	49	2.9	29
Co-R[WC-1]	0.01	1	0.03	58	16	95	5.6	15
Co-R[WC-3]	0.03	3	0.03	61	20	105	6.2	14
Co-R[WC-5]	0.05	5	0.03	57	20	85	5.0	18
Co-R[WC-7]	0.08	7	0.03	54	16	64	3.8	22
Co-R[WC-9]	0.10	9	0.03	49	18	47	2.8	29

[a] All catalyst samples were re-calcined at 300 °C in air for 2 h before TPR measurement.
[b] The reducibility was based on a calibration with Ag_2O (100% reducibility).
[c] Measurement error = ±5%.
[d] Error = ±5% of measurement of H_2 chemisorption.
[e] Co metal dispersion (%) = [2 × (total H_2 chemisorption/g_{cat})/(no. μmol Co tot./g_{cat})] × 100%.
[f] Average particle size (d_p) is based upon H_2 chemisorption and the amount of reduced cobalt [$d_p = 5/(S_{Co} \times \rho_{Co})$, where S_{Co} is the surface area of reduced Co/g of reduced Co, and ρ_{Co} is the density of cobalt]. Surface area occupied by one reduced Co atom assumed to be 6.62 Å^2 [27].
[g] The reducibility during TPR at 30–400 °C is related to the reducibility of the catalysts during standard reduction [6].

0.2 wt.% (61–76% of the carbon was removed). After TPR the same amount of carbon appeared to still remain for Co–R[C-9]. This suggests that the form of carbon left was graphite, which did not have an effect on the amount of H_2 consumed during TPR. However, for Co–R[WC-9], the amount of carbon removed during TPR was at most ca. 0.1 wt.%, and may have been zero given experimental error. Based on calculation,

Table 3
Reaction rate for CO hydrogenation on Co/γ-Al_2O_3 reduced at various reduction gas compositions

Catalyst samples	CO conversion (%)[a]		Rate (μmol/g_{cat} s^{-1})[b]		CH_4 selectivity (%)		$TOF_H \times 10^3$ (s^{-1})[c]	
	Initial[d]	SS[e]	Initial	SS	Initial	SS	Initial	SS
Co–R	1.1	0.8	1.1	0.8	93	94	10.0	7.4
Co–R[C-3]	2.0	1.4	1.9	1.3	84	85	8.1	5.6
Co–R[C-5]	5.8	4.6	5.5	4.4	86	76	23.0	18.0
Co–R[C-9]	0.7	0.6	0.7	0.5	96	92	2.6	1.9
Co–R[W]	0.9	0.5	0.8	0.5	84	82	8.2	5.1
Co–R[WC-3]	3.6	3.3	3.3	3.0	92	88	16.0	14.0
Co–R[WC-5]	3.3	2.7	3.0	2.5	85	84	18.0	15.0
Co–R[WC-9]	2.4	1.5	2.2	1.4	86	80	23.0	15.0

[a] CO hydrogenation was carried out at 220 °C, 1.8 atm, and H_2/CO = 10 (H_2/CO/He = 20/2/8 cm^3/min).
[b] Error = ±5%.
[c] Based on total H_2 chemisorption.
[d] After 5 min of reaction.
[e] After 5 h of reaction.

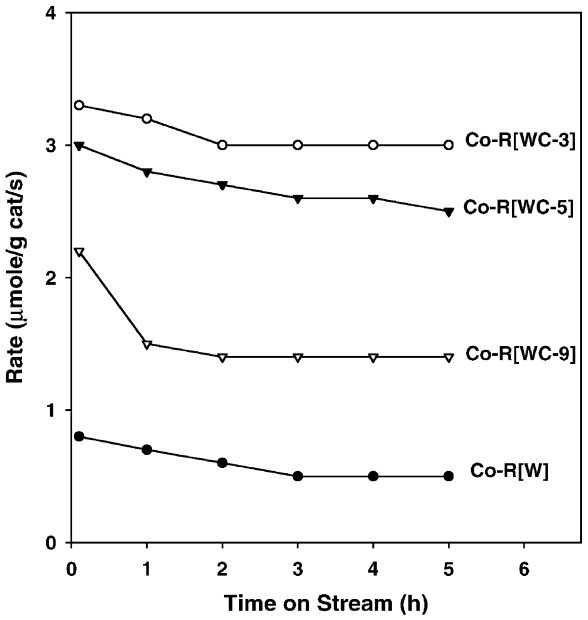

Fig. 10. Effect on reaction rate of CO addition during reduction at a high partial pressure of water vapor (ca. 23 mm Hg).

if 0.1 wt.% active carbon reacted with H_2 during TPR, this would account for at most only 3% of the total possible 100% reducibility for the 20 wt.% Co catalyst. This suggests that the pretreatment used prior to TPR measurement was able to remove most of the active carbon in the samples and any error introduced in the measurement of Co reducibility was minimal.

Besides Co reducibility, Co dispersion is critical in determining catalytic activity. There was an increase in Co dispersion upon CO addition during reduction (as determined by H_2 chemisorption) possibly because there was a decrease in sintering of the Co metal. However, the chemisorption results cannot be taken at face value. Clearly, if one looks at the values of TOF calculated, one sees a lot of variation. CO hydrogenation is well known to be a structure insensitive reaction. As such, TOF should not vary greatly with Co dispersion. If one considers the base samples (Co–R and Co–R[W]), their initial TOF's are ca. $1 \times 10^{-2}\,s^{-1}$—typical for Co catalysts under these conditions [25,26]. Since H_2 chemisorption on Co is highly activated, it must be carried out at 100 °C in order to come close to adsorbing hydrogen on all the available surface metal atoms in a reasonable time [19]. Reduction in the presence of added CO results in carbon deposition on the catalyst samples. Such carbon may bias the chemisorption results by (i) reacting with some H_2 to form CH_4, (ii) providing adsorption sites for H atoms that spill over from Co sites at 100 °C, and (iii) providing a bridge for H atoms to spill over onto the support. Any of these would, thus, result in an amount of hydrogen atoms "chemisorbed" greater than the number of reduced Co metal surface atoms. On the other hand, it is also possible that carbon could block some Co metal surface sites and, if spillover did not happen, would result in exposed Co metal sites being counted accurately. Although, based on steady-state isotopic transient kinetic analysis (SSITKA) results, it is known that the number of active intermediates on a Co surface during CO hydrogenation is only a small fraction of the number of Co metal surface atoms [25,26], this

Table 4
Carbon content on the Co catalysts after various pretreatments[a]

Catalyst samples	Carbon content (wt.%)[b]			
	After reduction (C–R–P)[c]	After re-reduction (C–R–P–R–P)[d]	After re-calcination (C–R–P–C)[e]	After TPR (C–R–P–C–TPR)[f]
Co–R[C-9]	0.86	0.37	0.21	0.20
Co–R[WC-9]	0.61	0.22	0.24	0.14

[a] C: calcination; R: reduction; P: passivation.
[b] Carbon content on the various pretreated catalyst samples was analyzed using combustion/coulometric titration by Galbraith Laboratories, Inc.
[c] Reduction of the calcined catalyst was done at 350 °C for 10 h with the various reduction gas mixtures.
[d] Re-reduction on the reduced catalyst was also done at 350 °C for 10 h with H_2.
[e] Re-calcination of the reduced catalyst was done at 300 °C for 2 h prior to TPR measurement.
[f] TPR was performed from 30 to 900 °C.

fraction remains fairly constant for a wide variety of Co dispersions. It can be suggested that Co–R[C-9] exhibited a large amount of hydrogen chemisorbed, but a low TOF based on its low rate. One might imagine that, for this sample at the highest concentration of added CO, spillover of hydrogen must have occurred. It should be noted that this catalyst also had the highest concentration of deposited carbon. All the rest of the samples gave reasonable TOF's (within a factor of 2, as is often seen [25]).

It should also be mentioned that XRD did not detect any difference upon CO addition during reduction. The XRD results are typical for reduced Co/γ-Al_2O_3 catalysts [6,18]. However, Raman spectroscopic results were clearly different. In our previous investigation of Co-SCF [18], it was found that Raman spectroscopy is one of the most powerful techniques besides TPR able to identify Co "aluminate" formation (two broad Raman bands at ca. 690 and 560 cm^{-1}). The identified Co "aluminate" is suggested to be different from $CoAl_2O_4$ (spinel) due to it being a non-stoichiometric surface Co "aluminate" compound. In the present study, dramatic changes in the characteristics of the Raman bands for the reduced and passivated catalyst samples were observed with the addition of CO during standard reduction. Basically, the Co "aluminate" bands disappeared more and more with increasing amount of CO added. The Raman bands for the passivated samples of apparently Co_3O_4 at 690 and 480 cm^{-1} became more dominant. This suggests that the addition of CO during reduction may have helped to decrease the amount of Co "aluminate" formed. It should be noted that the characteristics of Raman bands for Co–R[C-*n*] and Co–R[WC-*n*] were different. This is based on the fact that water vapor increases the amount of Co "aluminate" formed. Since Co catalysts in general and Co/Al_2O_3 in particular are not good water-gas shift catalysts [28–32], Co is not able to react significantly with the water to decrease its concentration.

It is clear that CO addition during reduction had effects on Co reducibility and dispersion of the catalyst samples. Based on all the evidence presented, it is suggested that the increase in specific activity (per gram basis) seen was primarily due to an increase in Co reducibility along with an increase in the number of Co metal surface atoms as determined by H_2 chemisorption.

5. Conclusions

The addition of CO during standard H_2 reduction of a 20% Co/Al_2O_3 catalyst produced specific activities about four times greater than when the catalyst reduced without CO addition. Most of this increase appears to have been due to increases in Co reducibility and dispersion. In general, initial and steady-state rates of CO hydrogenation, Co reducibility, and Co dispersion went through a maximum for 3–5 vol.% CO added during H_2 reduction. Carbon deposition was detected upon increasing the amount of added CO. The effect of CO addition may be due to one or more of possibly three reasons: (i) CO may help to prevent the formation of Co species strongly interacting with the support, thereby facilitating its reduction, (ii) CO may decrease sintering of the Co metal resulting an increase in Co dispersion, and (iii) CO may block Co "aluminate" formation by minimizing the impact of water vapor even at low partial pressures.

Acknowledgements

The authors would like to thank the Royal Thai government for financial support of BJ; Energy International, Inc. for providing the catalysts used in this study; and the Center for Advanced Engineering Fibers and Films (CAEFF) for the Raman spectrometer used in this study.

References

[1] H.P. Withers Jr., K.F. Eliezer, J.W. Mitchell, Ind. Eng. Chem. Res. 29 (1990) 1807.
[2] E. Iglesia, Appl. Catal. A. 161 (1997) 59.
[3] R.C. Brady, R.J. Pettit, J. Am. Chem. Soc. 103 (1981) 1287.
[4] A. Kogelbauer, J.C. Weber, J.G. Goodwin Jr., Catal. Lett. 34 (1995) 259.
[5] D. Schanke, A.M. Hilmen, E. Bergene, K. Kinnari, E. Rytter, E. Adnanes, A. Holmen, Catal. Lett. 34 (1995) 269.
[6] Y. Zhang, D. Wei, S. Hammache, J.G. Goodwin Jr., J. Catal. 188 (1999) 218.
[7] R. Riva, H. Miessner, R. Vitali, G.D. Piero, Appl. Catal. A. 196 (2000) 111.
[8] R. Bechara, D. Balloy, J.Y. Dauphin, J. Grimblot, Chem. Mater. 11 (1999) 1703.
[9] M. Kraum, M. Baerns, Appl. Catal. A 186 (1999) 189.
[10] B. Ernst, S. Libs, P. Chaumette, A. Kiennemann, Appl. Catal. A 186 (1999) 145.

[11] J.M. Jablonski, M. Wolcyrz, L. Krajczyk, J. Catal. 173 (1998) 530.
[12] B. Ernst, A. Bensaddik, L. Hilaire, P. Chaumette, A. Kiennemann, Catal. Today 39 (1998) 329.
[13] H. Ming, B.G. Baker, Appl. Catal. A 123 (1995) 23.
[14] D. Schanke, A.M. Hilmen, E. Bergene, K. Kinnari, E. Rytter, E. Adnanes, A. Holmen, Energy Fuels 8 (1996) 867.
[15] R.L. Chin, D.M. Hercules, J. Phys. Chem. 86 (1982) 360.
[16] L.B. Backman, A. Rautiainen, A.O.I. Krause, M. Lindblad, Catal. Today 43 (1998) 11.
[17] R.B. Greegor, F.W. Lytle, R.L. Chin, D.M. Hercules, J. Phys. Chem. 85 (1981) 1232.
[18] B. Jongsomjit, J. Panpranot, J.G. Goodwin Jr., J. Catal. 204 (2001) 98.
[19] R.C. Reuel, C.H. Bartholomew, J. Catal. 85 (1984) 63.
[20] A. Kogelbauer, J.G. Goodwin Jr., R. Oukaci, J. Catal. 160 (1996) 125.
[21] D. Schanke, S. Vada, E.A. Blekkan, A.M. Hilmen, A. Hoff, A. Holmen, J. Catal. 156 (1995) 85.
[22] P. Arnoldy, J.A. Moulijn, J. Catal. 93 (1985) 38.
[23] A.M. Hilmen, D. Schanke, A. Holmen, Catal. Lett. 38 (1996) 143.
[24] H.A. Bahr, V. Jessen, Ber. B 63 (2) (1930) 226.
[25] G.J. Haddad, B. Chen, J.G. Goodwin Jr., J. Catal. 161 (1996) 274.
[26] A.R. Belambe, R. Oukaci, J.G. Goodwin Jr., J. Catal. 166 (1997) 8.
[27] J.R. Anderson, Structure of Metallic Catalysts, Academic Press, New York, 1975.
[28] R.B. Anderson, Catalysis, in: P.H. Emmett (Ed.), Hydrocarbon Synthesis, Hydrogenation and Cyclization, vol. IV, Reinhold, New York, 1956, pp. 268–269.
[29] J.G. Goodwin Jr., in: Proceedings of the Symposium on Methane Upgrading, Preprints of the Division of the Petroleum Chemistry, vol. 36, 1991, p. 156.
[30] E. Iglesia, S.L. Soled, R.A. Fiato, G.H. Via, J. Catal. 143 (1993) 345.
[31] G.J. Haddad, Ph.D. Dissertation, University of Pittsburgh, 1995.
[32] R.J. Farrauto, C.H. Bartholomew, Fundamentals of Industrial Catalytic Processes, Blackie, New York, 1997, p. 388.